ELSEVIER

Small scale localization in turbulent flows. A priori tests applied to a possible Large Eddy Simulation of compressible turbulent flows

Daniela Tordella [a,*], Michele Iovieno [a], Silvano Massaglia [b]

[a] *Politecnico di Torino, Dipartimento di Ingegneria Aeronautica e Spaziale, C.so Duca degli Abruzzi 24, 10129 Torino, Italy*
[b] *Università degli Studi di Torino, Dipartimento di Fisica Generale, Via P. Giuria 1, 10125 Torino, Italy*

Abstract

A method for the localization of small scales in turbulent velocity fields is proposed. The method is based on the definition of a function f of the velocity and vorticity fields that reproduces a normalized form of the twisting-stretching term of the Helmholtz equation. By means of this method the equations of motion can be selectively filtered in regions that are rich in small scale motions. The method is applied through a criterion built on a statistical link between the function f and a local property of the turbulence that was derived from the analysis a homogeneous and isotropic high Reynolds number ($Re_\lambda = 280$) turbulence field. The localization criterion is independent of the subgrid scale model used in a possible Large Eddy Simulation carried out after the small scale localization is obtained. This extends the typology of possible applications to the analysis of experimental laboratory data. In case of compressible regimes, a second sensor that depends on the local pressure variation and divergence can be associated to the previous one in order to determine the eventual emergence of shocks. The capture of shocks is made possible by suppressing the subgrid terms where this second sensor indicates the presence of a shock.

A priori tests were carried out on the turbulent channel flow, $Re_\lambda = 180$ and 590, to validate the localization procedure in a highly inhomogeneous flow configuration. A second set of a priori test was carried out on a turbulent time decaying jet which initiates its evolution at Mach 5 and which reproduces a few hydrodynamical properties of high Reynolds number hypersonic jets which exist in the Universe.
© 2007 Elsevier B.V. All rights reserved.

1. Introduction

The Large Eddy Simulation method is surely going to be one of the most frequently used tools to predict the behavior of turbulent flows in many different physical and engineering applications. Turbulent flows in nature are characterized by very high Reynolds numbers. Consequently, any attempt to numerically solve the Navier–Stokes equations for such flows requires a great number of scales to be resolved. At present, the largest three-dimensional turbulence simulations have a resolution that allows a ratio between the largest and the smallest scale of about a thousand (see, for example, Kaneda and Ishihara 2006,

isotropic turbulence in a box, 4096^3 grid points [1]). Thus, in general, the large scales only of the flow can be accurately simulated and a Large Eddy Simulation (LES) approach is considered appropriate. An instance of these occurrences is that of astrophysical flows.

Astrophysical flows occur in very large sets of spatial scales and velocities. Typical velocities for outflows from the Sun and stars attain 200–400 km s^{-1} and form solar and stellar supersonic winds and jets; for outflows from collapsed objects, e.g., black holes, jets can reach the speed of light. Correspondingly, the spatial scales range from hundreds of Astronomical Units, for stellar outflows, up to hundreds of kiloparsecs for jets from Active Galactic Nuclei (AGNs in the following). The resulting Reynolds numbers exceed 10^{10}–10^{13}. Moreover, such flows are hypersonic, with Mach numbers that attain values of up to $\sim$50 in Herbig–Haro jets and $\sim$100–1000 in jets from AGNs, with

* Corresponding author.
  E-mail address: daniela.tordella@polito.it (D. Tordella).

the consequent formation of shocks. Three-dimensional DNS of astrophysical flows undergoing shear-layer instabilities can, nowadays and in a foreseeable future, capture just the behavior that occurs at the largest scales (e.g., Bodo et al. [2], Micono et al. [3]) but not the development of turbulent motions, which are very likely induced by the instabilities.

In this context, there are two conflicting requirements: (1) to capture discontinuities such as shock waves without the introduction of spurious oscillations, which requires a relatively high numerical dissipation, (2) the numerical algorithm should not damp the resolved turbulent structures, which requires a low numerical dissipation.

The problem of the reliable representation of small scales in compressible turbulent flow simulations has often been overlooked. It has often been assumed that numerical dissipation, implicit in upwind shock capturing numerical schemes, could simulate net energy transfer from larger to smaller scales. However, it has been shown, by Ducros et al. [4], that such an approach is not compatible with LES modeling due to the antithetic behavior of the high numerical viscosity which overwhelms the subgrid scale term effects.

Our aim is the development of a general method that allows the detection of small turbulence scales. In order to locate the small scales, we propose the introduction of a criterion based on the local structure of the vorticity field, in particular, on its twisting and stretching intensity. In such a way, it would be possible to selectively introduce a compressible sub-grid scale model (for example, the Smagorinsky Model evaluated by means of Favre-averaged quantities).

The criterion for the small scale localization, which is described in Section 2, is based on the introduction of a local function f of the vorticity and velocity gradient and on Morkovin's hypothesis (Morkovin [6]), which states that the essential dynamics of supersonic turbulence follows the incompressible pattern. Function f uses information from the stretching term in the vorticity equation, which is responsible for the generation of smaller scales. The behavior of the function is observed in a developed homogeneous and isotropic turbulence (HIT) field, either fully resolved, by means of direct numerical simulation (DNS, Biferale et al. [7], $Re_\lambda = 280$) or under-resolved, by means of a sequence of filtering operations carried out using different filter scales. The box filter has been used. A range of f typical values for the homogeneous and isotropic turbulence can be selected by means of a threshold t_ω and through the computation of the probability density distribution that function f is larger than a given threshold. The behavior of this threshold t_ω is observed through a priori tests on high-resolution, direct numerical simulation of incompressible homogeneous and isotropic turbulence. A link with a statistical local property of the turbulence is apparent. Values larger than a certain limit value cannot be observed if the field is fully resolved. This observation has been exploited to build the localization criterion.

An earlier instance of localization procedure was the Selective Structure-Function Model (SSF) developed in 1993 by M. Lesieur and collaborators (see, e.g., Lesieur and Metais [8]). In this study the idea was to switch off the turbulent viscosity when the flow is not sufficiently three-dimensional. Based on statistical data from Homogeneous Isotropic Turbulence, if the angle between the vorticity—at a given grid point—and the surrounding vorticity average exceeds a certain threshold (20 degrees), the eddy viscosity is settled. This threshold value results to depend on the resolution of the simulation, see again Lesieur and Metais [8].

In the present paper we propose a function f that, besides the twisting process, includes the stretching process. The discussion on the physical character and implications of function f is in Section 2. This new localization criterion does not depend on the simulation discretization. Before applying it to a priori tests concerning the implementation of the Large Eddy Simulation method to a highly inhomogeneous and anisotropic flow, such as a supersonic turbulent jet, we present a further evidence of the efficiency of the present localization criterion in the turbulent channel flow. This flow, in fact, can be considered the paradigm of inhomogeneous turbulent flows. The efficiency of the use of this criterion in wall turbulence is obtained by comparing the distribution of the probability that $f \geqslant t_\omega$ in the DNS of the turbulent channel flow at two values of Reynolds number ($Re_\tau = 180$ [9,10], $Re_\tau = 590$ [11]) and in few associated filtered fields where the small scales where removed, see Section 2.

The criterion was then applied to snapshots from a numerical simulation of the temporal decay of a hypersonic jet with an initial Mach number of 5 (according to Bodo et al. [2], Micono et al. [3], see also the review by Ferrari [13]), see Section 3.2. This has made it possible to identify the presence of small scales and then the region where it is opportune to filter the motion equations and insert a subgrid scale turbulence model. In such a way the compressible momentum balance is corrected by adding the contribution from the subgrid terms to the turbulent stresses. This improves the general properties of the jet—in particular, the spatial growth rate—obtaining values which agree well with the central value of available experimental determinations (see, e.g., Brown and Roshko [15], Lu and Lele [16], Slessor et al. [17], Smith and Dussage [18]). The concluding remarks are given in Section 4.

2. Small scale localization criterion

The criterion for small scale localization is based on the introduction of the function

$$f(\mathbf{u}, \boldsymbol{\omega}) = \frac{|\boldsymbol{\omega} \cdot \nabla \mathbf{u}|}{|\boldsymbol{\omega}|^2}, \tag{1}$$

where $\mathbf{u}$ is the velocity vector, and $\boldsymbol{\omega} = \text{curl} \, \mathbf{u}$ is the vorticity vector.

Function f is a normalized form of the vortex-stretching term in the Helmholtz equation. This term is responsible for the generation of vortical three-dimensional small scales. It can be observed that when the flow is three-dimensional and rich in small scales f is necessarily different from zero. In general, function f is zero in 2D vortical fields. When a mean steady or unsteady shear flow is present, f is different from zero. This also includes laminar flow configurations. To avoid this problem, the dependence of f from the mean field must

be removed by subtracting the mean field from the velocity and vorticity fields. In such a way a function f' that only depend on the fluctuation field can be introduced. Two formulation can be proposed, the first to be used in a field obtained from direct numerical simulation (DNS),

$$f'_{\mathrm{DNS}}(\mathbf{u}, \boldsymbol{\omega}) = \frac{|(\boldsymbol{\omega} - \overline{\boldsymbol{\omega}}) \cdot \nabla(\mathbf{u} - \overline{\mathbf{u}})|}{|\boldsymbol{\omega} - \overline{\boldsymbol{\omega}}|^2}, \qquad (2)$$

where $\overline{\mathbf{u}}, \overline{\boldsymbol{\omega}}$ are the average of the velocity and vorticity that are defined according to the space–time averaging introduced by Monin and Yaglom [21, Section 3.1]

$$\overline{\mathbf{g}} = \int_{-\infty}^{\infty} \int_{-\infty}^{\infty} \mathbf{g}(\mathbf{x} - \boldsymbol{\xi}, t - \tau)\psi(\boldsymbol{\xi}, \tau)\, \mathrm{d}\boldsymbol{\xi}\, \mathrm{d}\tau, \qquad (3)$$

where $\mathbf{g}$ is a generic physical quantity and $\psi(\boldsymbol{\xi}, \boldsymbol{\tau})$ is a weighting function which satisfy the normalization condition

$$\int_{-\infty}^{\infty} \int_{-\infty}^{\infty} \psi(\boldsymbol{\xi}, \boldsymbol{\tau})\, \mathrm{d}\boldsymbol{\xi}\, \mathrm{d}\tau = 1.$$

The second formulation is to be used when dealing with filtered fields coming from Large Eddy Simulations (LES)

$$f'_{\mathrm{LES}}(\langle \mathbf{u} \rangle, \langle \boldsymbol{\omega} \rangle) = \frac{|(\langle \boldsymbol{\omega} \rangle - \overline{\langle \boldsymbol{\omega} \rangle}) \cdot \nabla(\langle \mathbf{u} \rangle - \overline{\langle \mathbf{u} \rangle})|}{|\langle \boldsymbol{\omega} \rangle - \overline{\langle \boldsymbol{\omega} \rangle}|^2}, \qquad (4)$$

where $\langle \cdot \rangle$ indicated a filtered quantity. Again, quantities $\overline{\langle \mathbf{u} \rangle}$ and $\overline{\langle \boldsymbol{\omega} \rangle}$ are the mean of the filtered velocity and vorticity according to definition (3).

The above remarks suggest the use of f' as a potential local indicator of the presence of small scales in a 3D fluctuating field where the stretching-twisting process is active. This can made possible if a statistical link between the certainty of the presence of small scales (as in high Reynolds number Homogeneous Isotropic Turbulence) and special values of the function f' in such a flow can be found. To this end, a question can be asked. Are there values of f' which can/cannot be found in a highly developed turbulent field where the small scale are surely present and, which, vice versa, cannot/can be found in a coarser field as is the filtered field that is obtained from a LES?

In order to understand the behavior of f', with regards to the local property of a fully developed turbulent flow, f' is first observed in a fully resolved homogeneous and isotropic incompressible turbulence, then in a few under-resolved homogeneous-isotropic turbulences as well as in a turbulent inhomogeneous field, as it is the channel flow. In these fields, a typical range of f' values can be determined by considering a threshold t_ω and by computing the probability density distribution that f' is larger than a chosen value both in the resolved and under-resolved fields.

For this purpose, a priori tests have been carried out on a DNS of a homogeneous and isotropic turbulence (in the following called HIT, 1024^3 grid, $Re_\lambda = 280$, see Biferale et al. [7]) and on four box filtered fields with resolutions of $64^3, 128^3, 256^3$ and 512^3 deduced from this DNS. The 1024^3 turbulence is here considered a resolved fully developed turbulent field and is taken as a reference. The function f' is
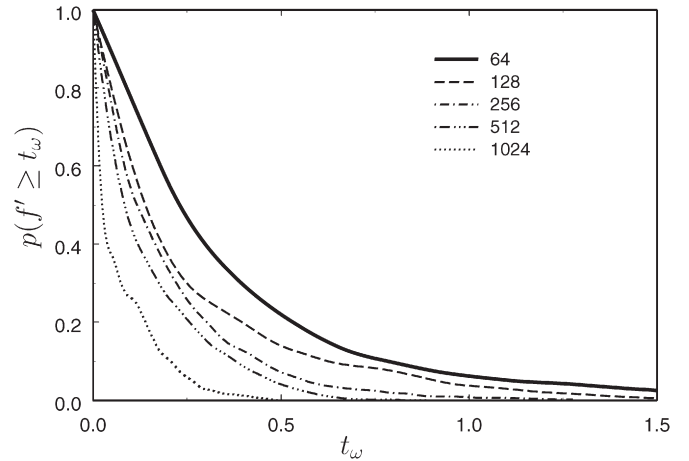

Fig. 1. Distribution of the probability of f' for different resolutions of incompressible homogeneous and isotropic turbulence (sensor f'_{DNS} for the resolution 1024^3, sensor f'_{LES} for the filtered fields).

computed for all the fields. As previously mentioned, the range of the possible f' values in a resolved HIT and in an under-resolved HIT can be obtained by considering a threshold t_ω and by computing the probability density distribution that f' is larger than the given value. In Fig. 1, it can be noticed that there is an almost zero probability of having $f' \geqslant t_\omega \approx 0.5$ in the resolved turbulence. This value can be regarded as the maximum stretching which a turbulent flow with a fine grain can yield. On the contrary, in the unresolved cases, larger values are possible, with a probability that is in $[0, 0.2]$. Thus, in theory, if in a simulation of a fully developed turbulent flow, f' assumes values larger than 0.5, the turbulent field should be considered under-resolved and should benefit from the local activation of the Large Eddy Simulation method (LES) by inserting a sub-grid scale term in the motion equation. In this way, we consider regions where f' is higher than t_ω as under-resolved regions where there should be scales that are smaller than the local filter scale and where the activation of a LES procedure is opportune.

It should be noticed that the value of t_ω, which gives an exactly zero $p(f' \geqslant t_\omega)$ is not numerically well determinable. It is opportune to fix a value that corresponds to a sufficiently small finite probability. We have considered that a threshold, where f' values with a probability of about 2 out of 100 can be allowed, can be reasonable. From the 1024^3 grid curve in Fig. 1, this yields $t_\omega \sim 0.40$ (that is, $p(f' \geqslant t_\omega) \sim 0.02$).

To verify the reliability of this proposal in a highly inhomogeneous turbulent field, we considered the direct numerical simulation of a turbulent channel flow at $Re_\tau = 180$ with a grid resolution of $(N_x, N_y, N_z) = (96, 128, 64)$ [9] and its filtered counterpart with a resolution of $(N_x, N_y, N_z) = (48, 65, 32)$ points in the streamwise, normal and spanwise directions, respectively, as well as the direct numerical simulations of a turbulent channel flow at $Re_\tau = 590$ with a grid resolution of $(N_x, N_y, N_z) = (384, 257, 384)$ [11] and its two filtered counterparts with resolution $(N_x, N_y, N_z) = (96, 129, 96)$ and $(N_x, N_y, N_z) = (192, 185, 192)$. We computed f'_{DNS}, relation (2), in the DNS fields and f'_{LES}, relation (4), in the filtered fields. Then, we compared the probability distributions that
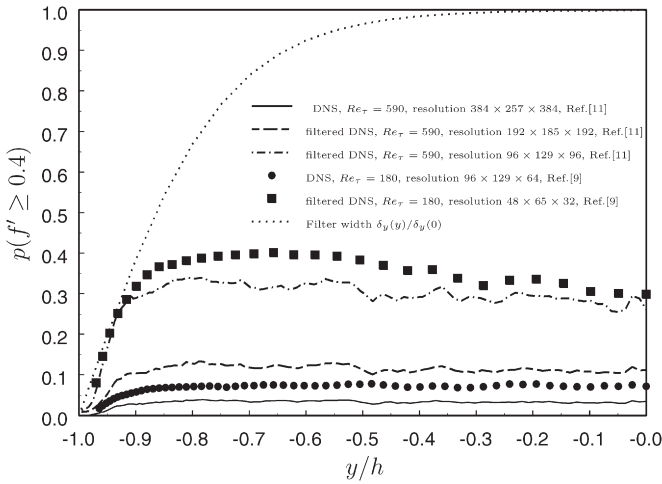
Fig. 2. Distribution of probability that $p(f' \geqslant 0.4)$ along the channel width. The filter is uniform in streamwise (x) and spanwise (z) directions, while it varies as an hyperbolic tangent in the wall normal direction y. The filter widths are: for the resolution $192 \times 185 \times 192$: $\delta_x/L_x = 0.01$, $\delta_z/L_z = 0.01$, $\delta_y(0)/h = 0.012$; for the resolution $96 \times 129 \times 96$: $\delta_x/L_x = 0.02$, $\delta_z/L_z = 0.02$, $\delta_y(0)/h = 0.025$; for the resolution $48 \times 65 \times 32$: $\delta_x/L_x = 0.04$, $\delta_z/L_z = 0.06$, $\delta_y(0)/h = 0.05$. The domain of all simulations is $L_x = 2\pi h$, $L_z = \pi h$, where h is the channel halfwidth. Probabilities at $Re_\tau = 590$ are computed using the instantaneous field available online at http://davinci.tam.uiuc.edu/data/moser/chandata (see [11]).

function $f \geqslant t_\omega$ across the channel in the highly resolved DNS fields and in the filtered fields. Fig. 2 shows these distributions. Once again it can be seen that the field which contains the smallest scales relevant to its proper Reynolds number shows a very low probability. In fact, in Fig. 2 one can see that the curve which represents the DNS field by Moser et al. [11] shows a probability as low as 0.03, i.e. of the order of the probability $p(f' \geqslant 0.4) \sim 0.02$ which is observed in the 1024^3 HIT. This small difference can be considered due to the numerical uncertainty, but also to the fact that the curve that represents this DNS field is not the result of a statistical average because one temporal instant only is available for this data base (see http://davinci.tam.uiuc.edu/data/moser/chandata, [11]). The DNS at $Re_\tau = 180$ shows a probability of about 0.06. This DNS has statistics in excellent agreement with other analogous DNS and with laboratory data, see also [10], but, according with the present criterion of subgrid scale localization, is not perfectly resolved. In fact, the value 0.06, though small, is definitely higher than the uncertainty threshold that we propose, that is a too a high value to be interpreted as exclusively due to the computational uncertainty. A posteriori, we think that the explanation is a non-sufficient resolution in the spanwise direction where we put 64 points only. Fig. 2 also shows that the filtered fields always have high values of the probability $p(f' \geqslant t_\omega)$. The lower the resolution the higher the probability, a fact that is in full agreement with what is observed in the Homogeneous Isotropic Turbulence, see Fig. 1, and which supports the proposed small scale localization criterion.

Underlying the present small scale localization criterion, is the hypothesis that the compressibility effects do not have much influence on the turbulence dynamics, apart from varying the local fluid properties (Morkovin [6], Duros et al. [4]).

3. Application to the time evolution of a highly compressible turbulent jet

3.1. Description of the test flows

Astrophysical jets are highly collimated supersonic flows that emerge from objects, such as neutron stars, Young Stellar Objects (YSOs) or the supermassive black holes that are thought to power the galactic nuclei. The mass accretion–ejection phenomenon is usually mediated by an accretion disk. According to this scheme, jets are accelerated via magneto-centrifugal processes in the vicinities of the accreting object. As previously mentioned, jets are usually hypersonic and, in many instances, relativistic and are subject to shear-layer (or Kelvin–Helmholtz) instabilities (see Ferrari [13] for a review).

We have studied numerically, and in Cartesian geometry, the temporal evolution of a 3D jet subject to periodicity conditions along the longitudinal direction. The flow is governed by the ideal fluid equations for mass, momentum, and energy conservation, in the non-relativistic limit (as appropriate for the case of Herbig–Haro jets)

$$\frac{\partial \rho}{\partial t} + \nabla \cdot (\rho \mathbf{v}) = 0, \tag{5}$$

$$\rho \left[\frac{\partial \mathbf{v}}{\partial t} + (\mathbf{v} \cdot \nabla) \mathbf{v} \right] = -\nabla p, \tag{6}$$

$$\frac{\partial p}{\partial t} + (\mathbf{v} \cdot \nabla) p - \Gamma \frac{p}{\rho} \left[\frac{\partial \rho}{\partial t} + (\mathbf{v} \cdot \nabla) \rho \right] = 0, \tag{7}$$

where the fluid variables p, ρ and $\mathbf{v}$ are, as customary, the pressure, density, and velocity, respectively; $\Gamma (= 5/3)$ is the ratio of the specific heats.

The initial flow structure is a cylindrical jet in the 3D domain $\{(0, D) \times (-R, R) \times (-R, R)\}$, described by a Cartesian coordinate system (x, y, z). The initial jet velocity is along the x-direction; its symmetry axis is defined by $(y = 0, z = 0)$. The initial jet velocity, at $t = 0$, is $V_x(y, z) = V_0$ within the jet, i.e. for $(y, z) \leqslant a$, where a is the initial jet radius, and $V_x(y, z) = 0$ elsewhere. The initial particle density is set to $\rho(y, z) = \rho_0$ within the jet and $\rho(y, z) = \nu \rho_0$ outside, with ν the initial density ratio of the external medium to jet proper. Finally, we assume that the jet is initially in pressure equilibrium with its surroundings; for this reason, we assume an initially uniform pressure distribution p_0.

In the following, we will express lengths in units of the initial jet radius a, times in units of the sound crossing time of the radius a/c_0 (with $c_0 = \sqrt{\Gamma p_0/\rho_0}$), velocities in units of c_0 (thus coinciding with the initial Mach number), densities in units of ρ_0 and pressures in units of p_0.

This initial configuration is then perturbed at $t = 0$. The particular functional form of this perturbation is such as to excite a wide range of modes. Thus, we impose a superposition of longitudinally periodic transverse velocity disturbances, using the functional forms

$$v_y(x, y, z) = V_{y,0} \sum_{n=1}^{n_0} \sin(n k_0 x + \phi_n), \tag{8}$$

$$v_z(x, y, z) = V_{y,0} \sum_{n=1}^{n_0} \cos(nk_0 x + \phi_n), \qquad (9)$$

where $V_{y,0} = 0.01V_0$ and $\{\phi_n\}$ are the phase shifts of the various Fourier components. These perturbations are therefore a superposition of a fundamental mode, plus a number of its harmonics. This form also allows us to choose n_0 harmonics. In the following, we have used the value $n_0 = 8$; this value is sufficiently small for the shortest wavelength mode excited to still be accurately followed in time (i.e. to be adequately resolved) by our calculations.

The wavelength of the fundamental mode is set equal to the length of the computational domain; thus, $k_0 = 2\pi/D$, therefore if we set $k_0 = 0.2$, $D = 10\pi$. The shortest perturbation wavelength, $2\pi n_0/k_0$, is fixed by the maximum value of $n = n_0$, which—as already mentioned—is set at $n_0 = 8$. It is essential to note that the fundamental mode (of wavelength D) does not necessarily coincide with the most unstable mode; the wavelength of the most unstable mode depends on the actual values of the parameters that characterize the initial state of the jet.

We cover our integration domain ($0 \leqslant x \leqslant D$, $-R \leqslant y \leqslant R$, $-R \leqslant z \leqslant R$) by a 128^3 or 256^3 grid, with $R = 6$. We have adopted free boundary conditions at the outer y and z boundaries ($y = \pm R$, $z = \pm R$), that is, the gradient of each variable is set to zero at these boundaries, while periodic boundary conditions have been imposed in the longitudinal direction x. The main control parameters of this problem are the initial flow Mach number $M \equiv V_0/c_0$ and the density ratio ν.

The hydrodynamic equations (4), (5) and (6), supplemented with the previously described initial and boundary conditions, were solved using the PLUTO code (described in [14] and in http://plutocode.to.astro.it). This Godunov-type code supplies a series of high-resolution shock-capturing schemes that are particularly suitable for the present application. In order to discretize the Euler equations, we chose a version of the Piecewise-Parabolic-Method (PPM) [19], which is third-order accurate in space and second-order in time.

A visualization of the instantaneous vorticity field of the jet and of its typical anisotropy—with an initial Mach number $M = 5$ and $\nu = 10$—in a section placed 5π diameter downstream of the inlet at almost 13 time scales from $t = 0$ is shown in Fig. 3. Fig. 4(a) illustrates the representation of the temporal distributions of the averaged stream-wise velocity component U, while Fig. 4(b) shows the averaged stream-wise velocity U_a, the speed of sound c_a and the Mach number M_a computed in the axis of the jet. The space averaged streamwise velocity U and the mean axial velocity U_a can be calculated by applying (3) with a weighting function $\psi(\boldsymbol{\xi}, \tau) = \frac{1}{D}\delta(\xi_y)\delta(\xi_z)\delta(\tau)$,

$$U(y, z, t) = \int_{-\infty}^{\infty} \int_{-\infty}^{\infty} v_x \psi \, d\boldsymbol{\xi} \, d\tau = \frac{1}{D} \int_0^D v_x \, d\xi_x,$$

$$U_a(t) = U(0, 0, t), \qquad (10)$$

because the flow is statistically homogeneous in the x-direction. The velocity field $\mathbf{v}$ is interpreted as a filtered velocity field
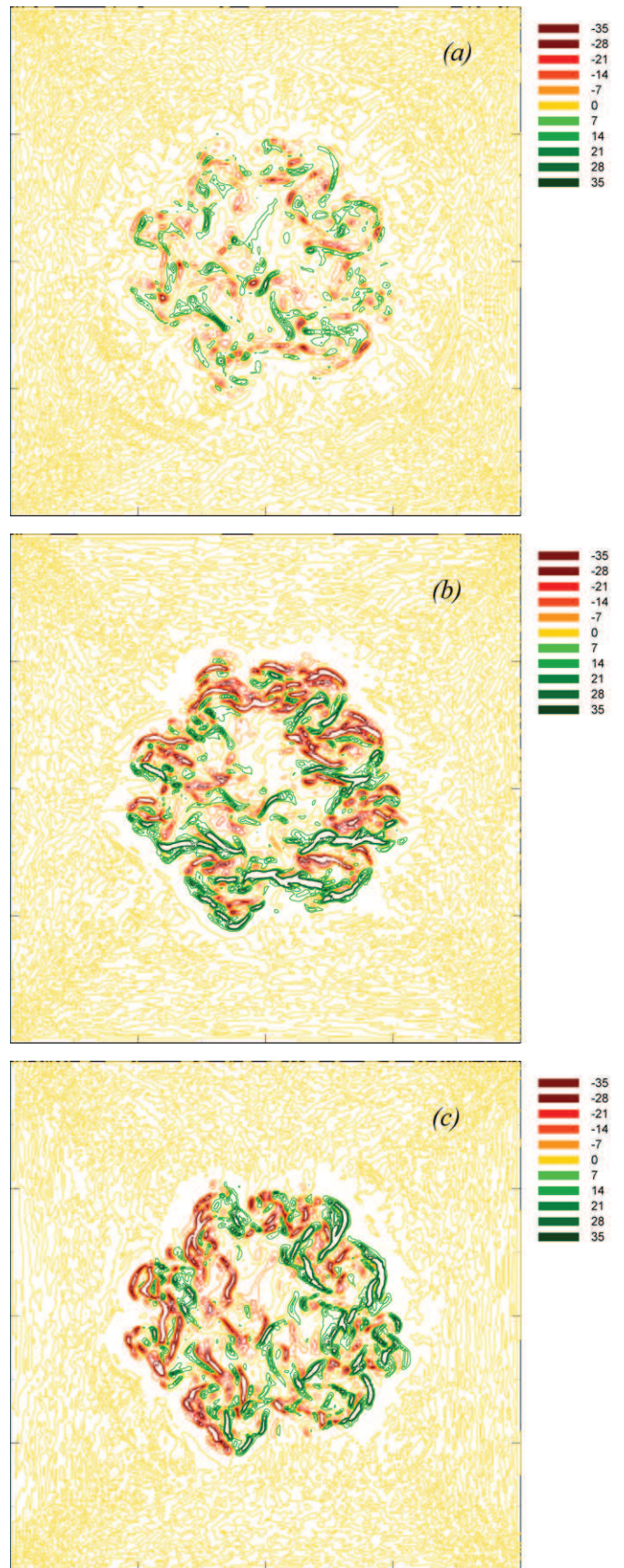

Fig. 3. Contour plot of the vorticity components, (a) w_x, (b) w_y, (c) w_z, in the middle section of the jet, $M = 5$, $t = 12.7$ time units.
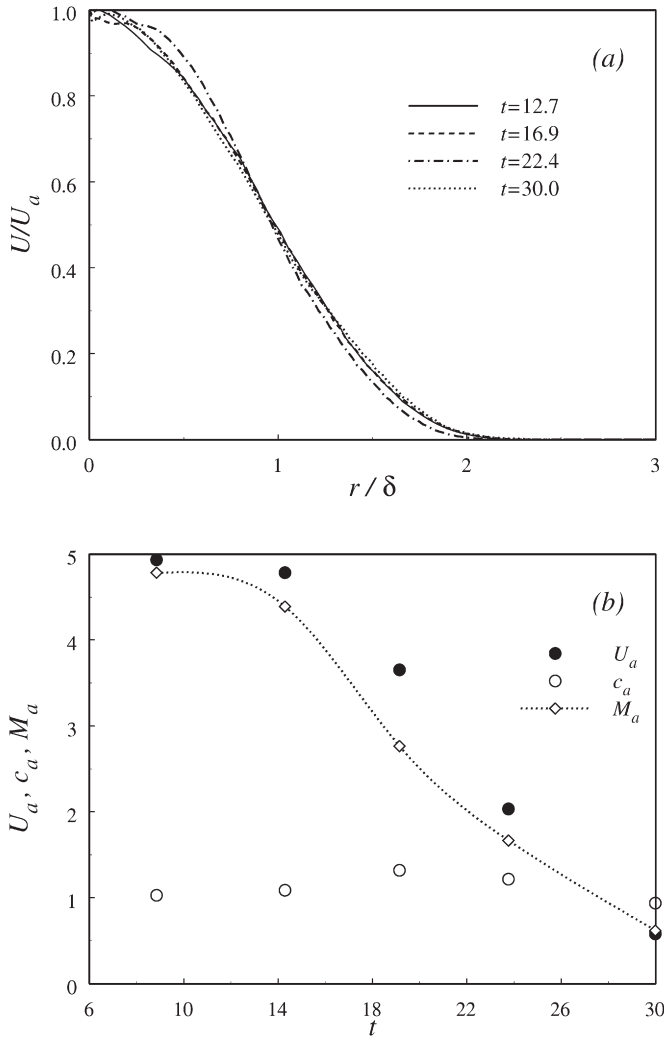
Fig. 4. Radial (a) and axial (b) distributions of the ensemble average of the longitudinal velocity. U is the average of longitudinal velocity, c is the speed of sound, M is the Mach number, suffix a stands for the centre of the jet and δ is the instantaneous jet thickness.

$\langle \mathbf{u} \rangle$ on the resolution defined by the computational grid of the pseudo-direct numerical simulation.

3.2. A priori tests

Fig. 5 shows the contour lines of the function $f'_{\text{LES}} = 0.4$ in longitudinal sections at $z = 0$ of the jet at different times and at two grid resolutions—128^3 and 256^3 points—of the Euler simulations. These are to be considered unresolved given that the Reynolds number of the real jets is of the order of 10^{10-13} and given that the previous resolutions allow no more than 10^3 as Reynolds number. We call these simulations pseudo-DNS and interpret them as LES fields. Since this pseudo-DNS is interpreted as a LES field, no explicit filtering is applied. Regions where f'_{LES} assumes larger values than 0.4 have been filled in black in Figs. 5 and 6. According to the present criterion, these can be viewed as regions where small scales are present and are under-resolved. Fig. 7 shows the fraction, along lines parallel to the x-direction, of the space occupied by the subgrid-scales

which is obtained using two different thresholds ($t_\omega = 0.2$ in part (a), $t_\omega = 0.4$ in part (b)) in the simulation 256^3. The core of the jet is on average richer of small scales, but it can be seen that the highest fraction values are found in spots that are scattered over the central part of the jet.

The temporal decay can be observed in the present jet simulation. The spatial longitudinal evolution is, on average, inhibited by the presence of periodicity boundary conditions. However, the associated spatial spreading rate can be estimated by applying Taylor's transformation and by computing the temporal spreading $\mathrm{d}\delta(t)/\mathrm{d}t$ of the simulated jet

$$\frac{\mathrm{d}\delta}{\mathrm{d}x} = \frac{\mathrm{d}\delta}{\mathrm{d}t}\frac{\mathrm{d}t}{\mathrm{d}x} = \frac{1}{U_a}\frac{\mathrm{d}\delta}{\mathrm{d}t}, \tag{11}$$

where $U_a = U_a(t)$ is the average of the longitudinal velocity on the axis of the jet, see Eq. (10). It can be noted that the ensemble averaged field is time dependent and axisymmetric.

Changing the coordinate system from Cartesian to cylindrical polar ($x =$ distance along the axis, $r =$ distance from axis, $\phi =$ azimuthal angle about the axis), let us indicate the instantaneous velocity components with v_x, v_r, v_ϕ and the ensemble averages with an overbar.

Along the temporal decay of the jet, for times larger than a few time scales, it is reasonable to assume that near (intermediate) similarity conditions have been reached, see Barenblatt [20]. Let us therefore consider filtering the instantaneous flow field, according to the general requirements of the Large Eddy Simulation method, see Germano [12]. The similarity hypothesis and axi-symmetry imply that the ensemble average of the filtered longitudinal velocity is of the kind $\langle v_x \rangle = U_a(t) f(\eta)$, where $\eta = r/\delta(t)$ is taken as the similarity variable.

In this situation, the ensemble averaged longitudinal momentum balance for the filtered field yields

$$\frac{\partial \overline{\langle v_x \rangle_F}}{\partial t} = -\frac{\partial \overline{\langle v_x \rangle_F \langle v_r \rangle_F}}{\partial r} - \frac{\overline{\langle v_x \rangle_F \langle v_r \rangle_F}}{r} + \frac{\partial \overline{\tau_{xr}^{sgs}}}{\partial r} + \frac{\overline{\tau_{xr}^{sgs}}}{r}, \tag{12}$$

where $\overline{\tau_{xr}^{sgs}} = \overline{\langle v_x \rangle_F \langle v_r \rangle_F} - \overline{\langle v_x v_r \rangle_F}$ is the ensemble average of the subgrid scale turbulent stress and the upperscript sgs stands for subgrid scale. The symbol $\langle \cdot \rangle_F$ represents Favre's filter operator ($\langle \rho \rangle \langle \cdot \rangle = \langle \rho \cdot \rangle$). The convective term on the right-hand side of (12), namely, the resolved convection term $-\overline{\langle v_x \rangle_F \langle v_r \rangle_F}$, is usually called resolved turbulent stresses. The total Reynolds stress is thus the sum of the resolved stress and of the subgrid scale stress. If a similarity transformation is now considered, the total Reynolds stress can be written as

$$-\overline{\langle v_x \rangle_F \langle v_r \rangle_F} + \overline{\tau_{xr}^{sgs}} = \overline{\tau_0^T}(t)g(\eta), \tag{13}$$

where $\overline{\tau_0^T}$ is a reference value for the total stress distribution (here chosen as the maximum value of the distribution). By inserting these similarity transformations in the longitudinal ensemble averaged balance, it can be deduced that

$$f(\eta) - \frac{\delta'(t)U_a(t)}{\delta(t)U_a'(t)}\,\eta f'(\eta) = \frac{\overline{\tau_0^T}(t)}{\delta(t)U_a'(t)}\left[g'(\eta) + \frac{g(\eta)}{\eta}\right]. \tag{14}$$

where the prime denotes both t and η derivatives. If the solutions f and g are of the assumed form, this equation must
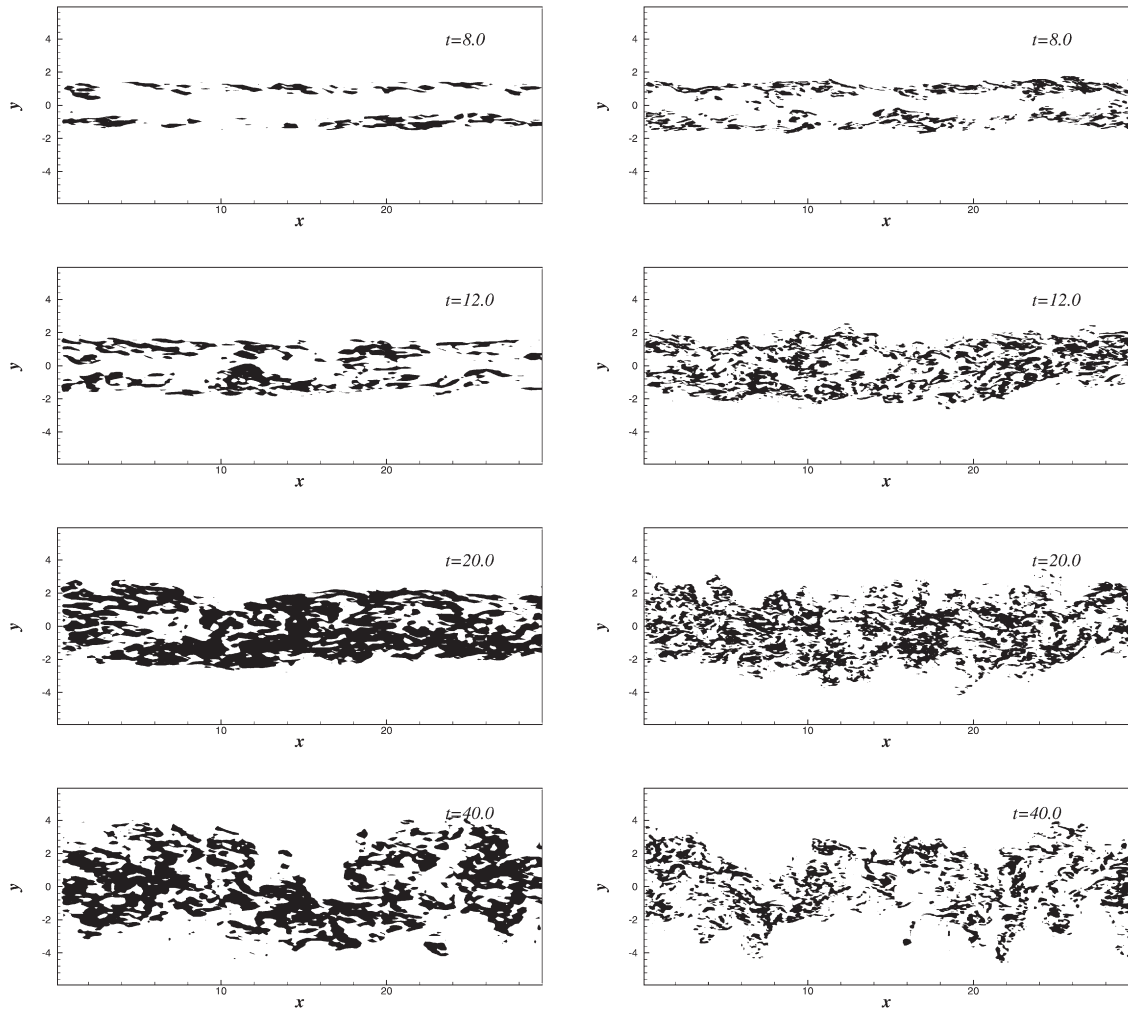
Fig. 5. Contour plots of the small scale functional $f'_{\text{LES}}(t_\omega = 0.4)$ in longitudinal sections $z = 0$ at different decay times. Left column: simulation with 128^3 grid points, right column: simulation with 256^3 grid points.

reduce to a total differential equation in f and g as a function of η; i.e. to exclude a dependence on the time variable t the two coefficients must be constant, therefore one obtains

$$\delta'(t)U_a(t) \propto \overline{\tau_0^T(t)}, \tag{15}$$

that is, the spreading rate is proportional to the total Reynolds stress.

If we now interpret the under-resolved Euler DNS ("pseudo-direct-simulation", Lesieur and Metais [8]) as a realization of the resolved field which could be obtained from a Large Eddy Simulation (i.e. without directly introducing the subgrid terms into the motion equation), it is possible to write

$$\delta'_{pds}(t)U_{0\text{-}pds}(t) \propto \overline{\tau_{0\text{-}pds}^T(t)}, \tag{16}$$

where the subscript *pds* stands for pseudo-direct simulation. By dividing the left- and right-hand sides of relation (15) by the corresponding sides of (16), the compressible sub-grid correction to the spreading rate is obtained:

$$\frac{\mathrm{d}\delta}{\mathrm{d}t} = \left(\frac{\mathrm{d}\delta}{\mathrm{d}t}\right)_{pds} \frac{\overline{\tau_0^T}}{\overline{\tau_{0\text{-}pds}^T}}. \tag{17}$$

From (11) and (17), it is possible to estimate the correction of the spreading rate due to the introduction of the sub-grid terms in the simulation. The subgrid scale contribution to the turbulent stress, which is shown in Fig. 8(a), depends on the value of t_ω, since the subgrid terms are included in the regions where $f \geqslant t_\omega$. We have here used the Favre-averaged Smagorinsky model, that is the Smagorinsky model evaluated with Favre-averaged velocity, with Lilly's constant $C_s = 0.18$.

The spatial growth rate—the global parameter on which we estimate the improvement related to the use of the LES method—is a function of the global Mach number and density ratio ν. Experiments on jets or on plane mixing layers were collected in the famous "Langley curve", see, e.g., Smits and Dussage ([18], cf. par. 6.3, Fig. 6.2)—a set of data that collects information from different experiments both with planar and axi-symmetric geometry (see, for instance, Ikawa and Kubota [22], Maydew and Reed [23], Siriex and Solignac [24], Brown and Roshko [15])—but also in the papers by Lu and Lele [16], Slessor et al. [17], among others. For comparison purposes, we considered the data collected in Fig. 4 by Slessor et al. where the normalized compressible shear-layer growth rate
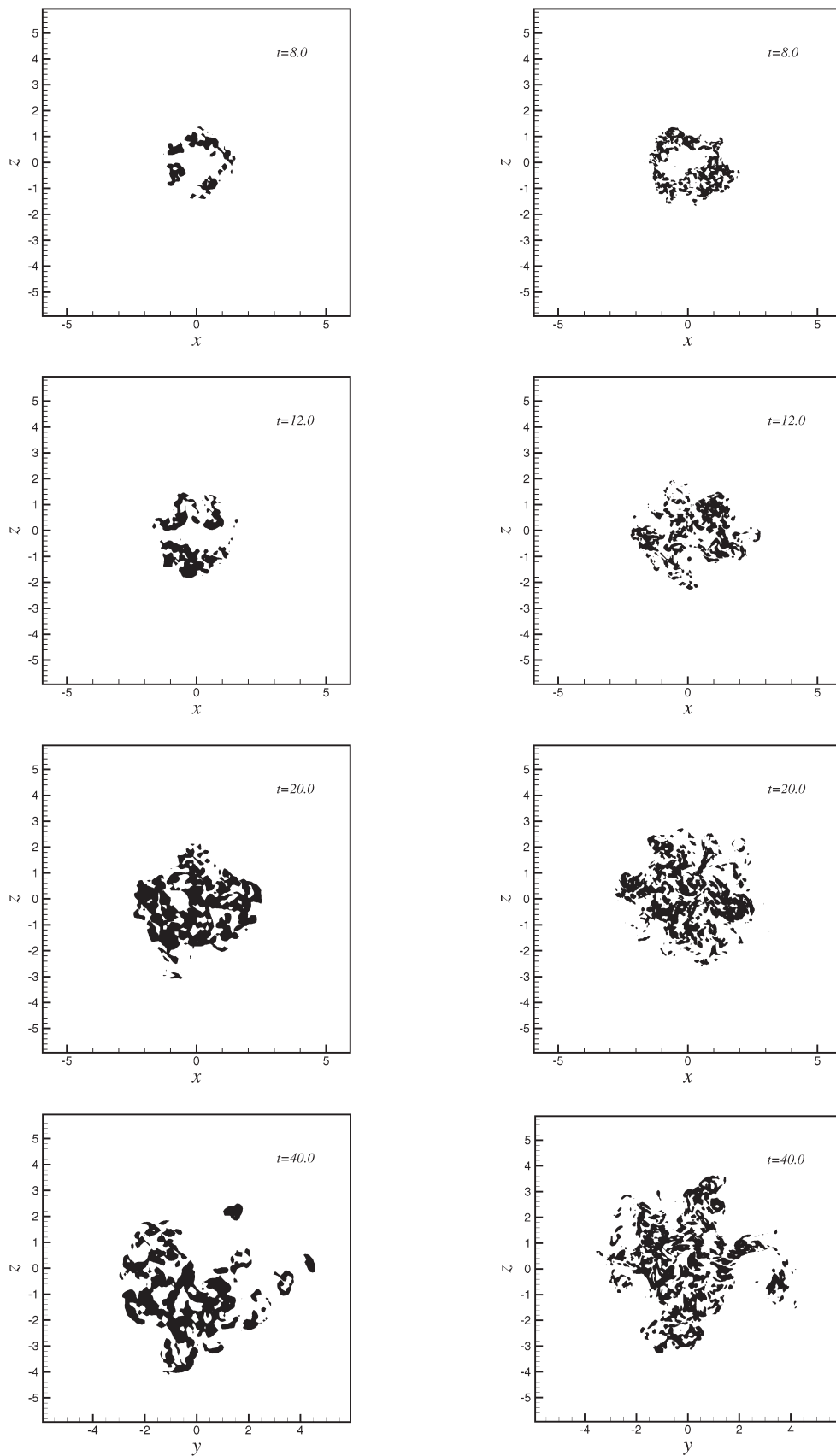
Fig. 6. Contour plots of the small scales functional $f'_{\text{LES}}(t_\omega = 0.4)$ in the middle transversal section at different decay times. Left column: simulation with 128^3 grid points, right column: simulation with 256^3 grid points.
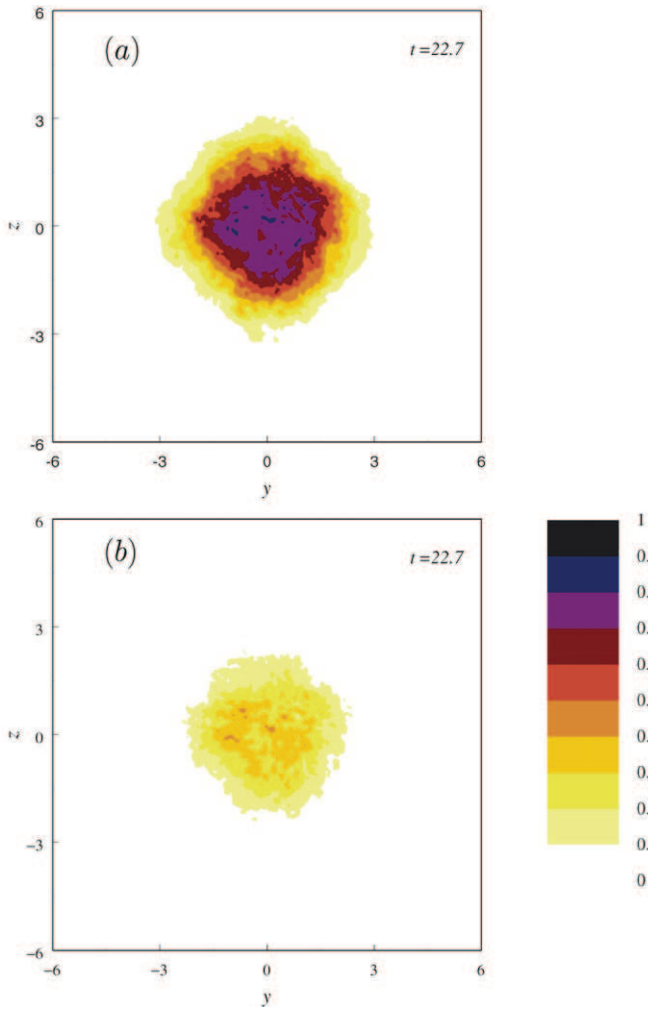
Fig. 7. Fraction of space where sub-filter scales are present according to a selected threshold t_ω on the functional f'_{LES}: (a) $t_\omega = 0.2$, (b) $t_\omega = 0.4$. Simulation 256^3, $t = 22.7$.

dependence on the compressibility parameter

$$\Pi_c = \max_{(i=1,2)} \left[\frac{1 - \Gamma_i}{a_i} \right] \Delta U \tag{18}$$

is shown. ΔU is here the difference of the mean longitudinal speed in the jet and outside the jet, index $i = 1, 2$ represents the gases inside and outside the jet, and Γ_i is the isentropic coefficient. Parameter Π_c is a parameter that exhibits a much-improved collapse with respect to the convective Mach number, and accounts for the observed systematic deviations in flows with extreme density/speed-of-sound ratios, see Lu and Lele [16] where these experimental deviations are considered to be due to an overestimation of the incompressible mixing growth rate. Let us recall that we actually have a very high density ratio, equal to about 10. Fig. 8(b) shows the correction obtained varying t_ω for two simulation resolutions. It can be observed that, when $t_\omega \sim 0.4$, the corrected value of the spatial spreading rate of the decaying jet (for example, when $M_a \sim 2.3$ and $\nu = 10$) comes very close to the experimental value at the same M_a that can be extrapolated from Figs. 4 and 5 by Slessor et al. [17] and from Fig. 14 by Brown and Roshko [15], which accounts for
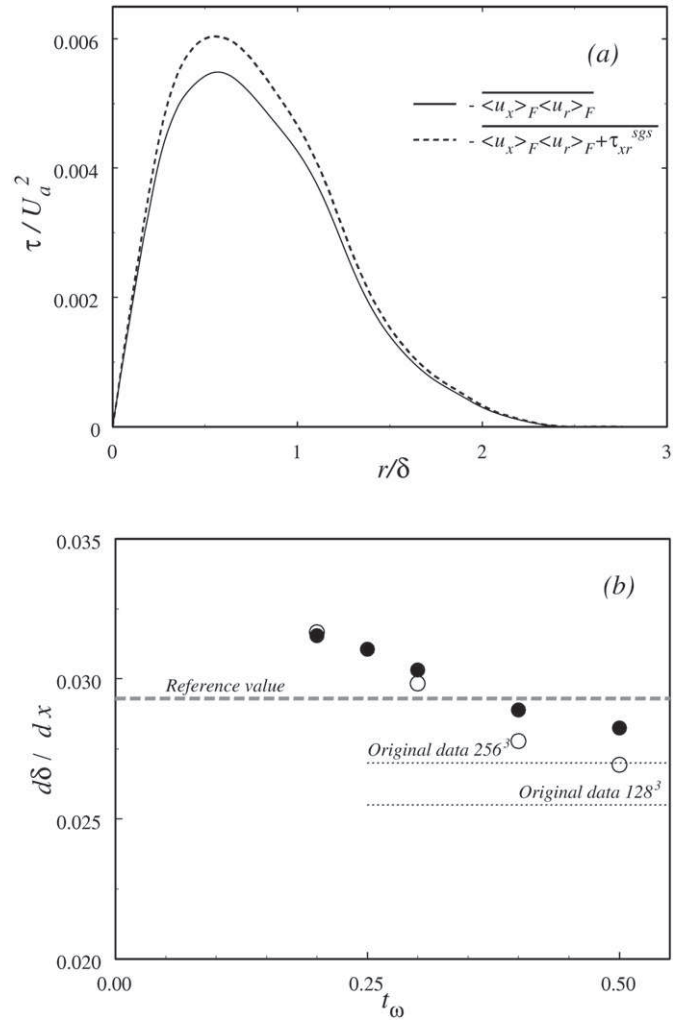

Fig. 8. (a) Transversal distributions of the Reynolds stress, with and without the subgrid scale contribution, simulation 256^3, $t_\omega = 0.3$, U_0 is the ensemble average of the longitudinal velocity, see definition (10). (b) Dependence of the correction on the spatial growth rate on t_ω, two different resolutions: filled circles 256^3, empty circles 128^3. Reference experimental value from Brown and Roshko [15] and Slessor et al. [17].

the effects associated to the high value of density ratio. This is in agreement with the contents of section two. It should be noticed that the correction does not depend to any great extent on the resolution of the simulation.

3.2.1. Shocks localization

As far as the shock localization is concerned, a vector sensor can be conceived in the form of a function

$$s_j = \alpha \beta_j, \qquad \alpha = \frac{(\nabla \cdot \langle \mathbf{u} \rangle)^2}{(\nabla \cdot \langle \mathbf{u} \rangle)^2 + \langle \omega \rangle^2},$$

$$\beta_j = 4 \left| \frac{\langle p \rangle_{j+1} - 2 \langle p \rangle_j + \langle p \rangle_{j-1}}{\langle p \rangle_{j+1} + 2 \langle p \rangle_j + \langle p \rangle_{j-1}} \right| \tag{19}$$

that in principle should multiply the explicit artificial dissipation terms in the discretized balance equations (e.g. Ducros et al. [4], Yee et al. [5]). Strong compressions are present when function s_i is of order 1. The identification of the regions where the shocks are present will then coincide with setting off the
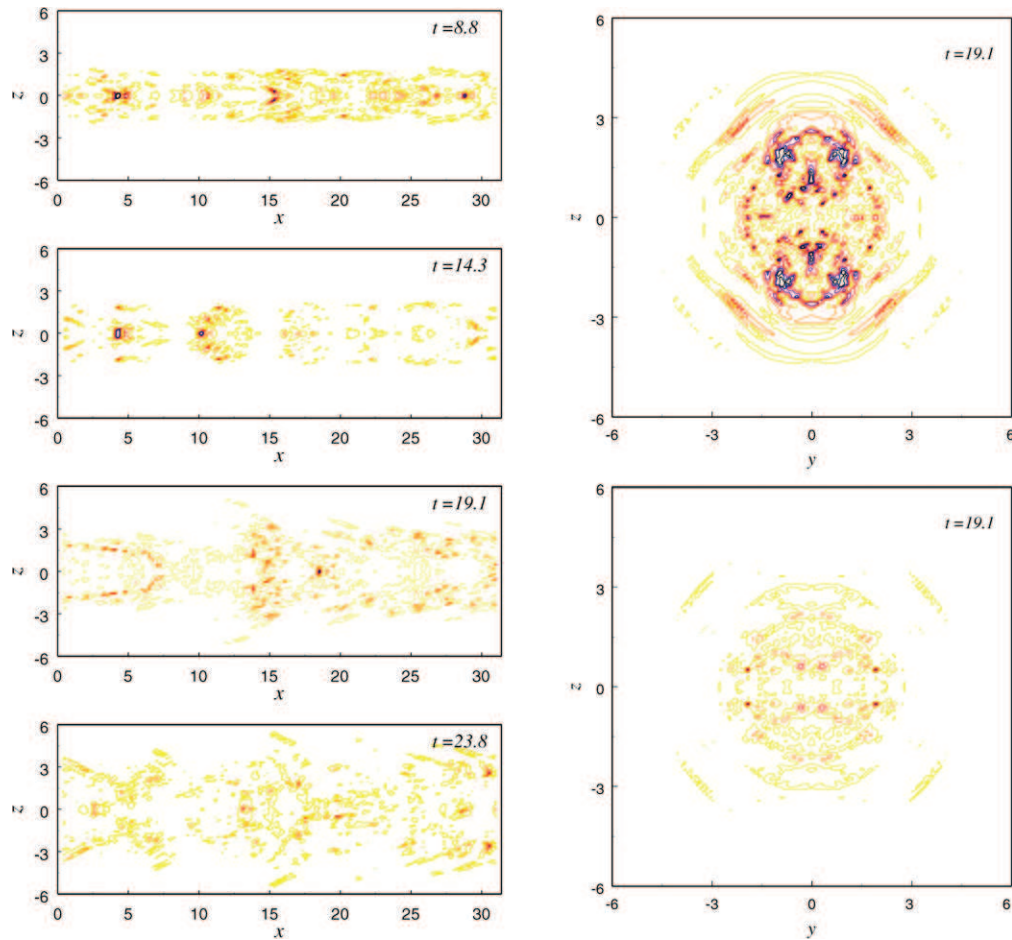
Fig. 9. Contour plots of the vector shock sensor $|s_j|$. Left column: longitudinal sections at different decay times, 128^3 grid points, right column: transversal sections at $x/D = 0.44$ and $x/D = 0.5$, 128^3 grid points. Mach number in the centre of the jet decays from 4.78 to 1.67.

numerical artificial dissipation and setting aside the subgrid scale model. This can be accomplished by structuring the Euler pseudo-direct-simulation equations with terms of the kind

$$s D_a + (1 - s) H(f - t_\omega) \nabla \cdot \tau^{sgs}, \tag{20}$$

where D_a means artificial dissipation. It should be noticed that in case of simulations which have an intrinsic numerical dissipation, as it is actually the present application, only the second term of (20) should be introduced in the governing equation. As an example, Fig. 9 shows the longitudinal and transversal contour levels at different simulation times of the modulus of s_j, for the jet simulation with the 128^3 spatial discretization.

4. Final remarks

A criterion of small scale localization, see sensors (2), (4), was built on the calculus of the local normalized modulus of vorticity stretching-twisting. This function is statistically linked to a local properties of the turbulence, which was derived from a high $Re_\lambda(280)$ Homogeneous and Isotropic Turbulence. The criterion is independent of the subgrid scale model used in any possible Large Eddy Simulations carried out after the small scale localization is obtained.

A priori tests were carried out in the turbulent channel flow ($Re_\tau = 180$ and $Re_\tau = 590$) and in a turbulent time decaying jet which initiates its evolution at Mach 5. The channel test shows the capability of the criterion to locate small scales in a highly

A global flow parameter—the spatial growth rate—was used to check the improvement introduced into a low resolution Euler simulation of a highly compressible jet carried out by implementing the LES method in the regions—determined using sensor (4)—where the density of small scale is high. The check was performed through a comparison with experimental outcomes from compressible mixings. This a priori test shows that a correction for the presence of small scales increases the spreading rate of the jet towards the experimental central value. By coupling the method of small scale localization here described to a procedure of shock localization, a possible tool to describe the interaction between shocks and large-scale turbulence structures can be obtained.

The computation of sensors (2), (4) and (19) does not depend on the mesh structure, vice versa these sensors could be of help to obtain a dynamic adaptation of the mesh to the flow. The implementation of sensors that are able to detect subgrid scales, independently of the use and the kind of subgrid scale model, is generally useful to study turbulence dynamics and can also be applied to analyze laboratory data. Furthermore, it allows LES

of complex flows to be obtained without a priori assumptions of the flow structure. The local character of such functions should allow easy parallelization.

Acknowledgements

References

[1] Y. Kaneda, T. Ishihara, High-resolution direct numerical simulation of turbulence, Journal of Turbulence 7 (20) (2006) 1–17.

[2] G. Bodo, P. Rossi, S. Massaglia, Three-dimensional simulations of jets, Astron. Astrophys. 333 (1998) 1117–1129.

[3] M. Micono, G. Bodo, S. Massaglia, P. Rossi, A. Ferrari, R. Rosner, Kelvin–Helmholtz instabilities in three-dimensional radiative jets, Astron. Astrophys. 360 (2000) 795–808.

[4] F. Ducros, V. Ferrand, F. Nicoud, C. Weber, D. Darracq, C. Gacherieu, T. Poinsot, Large-eddy simulation of the shock-turbulence interaction, J. Comp. Phys. 152 (1999) 517–549.

[5] H.C. Yee, N.D. Sandham, M.J. Djomehri, Low-dissipative high-order shock-capturing methods using characteristic-based filters, J. Comp. Phys. 150 (1999) 199–238.

[6] M.V. Morkovin, Effects of compressibility on turbulent flows, in: A. Favre (Ed.), Mècanique de la turbulence, 1961, p. 367.

[7] L. Biferale, G. Boffetta, A. Celani, A. Lanotte, F. Toschi, Particle trapping in three-dimensional fully developed turbulence, Phys. Fluids 17 (2) (2005), 021701/1–4.

[8] M. Lesieur, O. Metais, New trends in large eddy simulations of turbulent flows, Annu. Rev. Fluid Mech. 28 (1996) 45–83.

[9] M. Iovieno, G. Passoni, D. Tordella, A new large-eddy simulation near-wall treatment, Phys. Fluids 16 (11) (2004) 3935–3944.

[10] M. Iovieno, G. Passoni, D. Tordella, Vorticity fluctuation in the LES of the channel flow through new wall condition and the noncommutation error procedure, in: H.I. Andersson, P.A. Krogstad (Eds.), Advances in Turbulence, vol. 10, CIMNE, Barcelona, 2004, pp. 245–248.

[11] R.D. Moser, J. Kim, N.N. Mansour, Direct numerical simulation of turbulent channel flow up to $Re_\tau = 590$, Phys. Fluids 11 (4) (1999) 943–945.

[12] M. Germano, Turbulence, the filtering approach, J. Fluid Mech. 236 (1992) 325–336.

[13] A. Ferrari, Modeling extragalactic jets, Annu. Rev. Astron. Astrophys. 36 (1998) 539–598.

[14] A. Mignone, G. Bodo, S. Massaglia, T. Matsakos, O. Tesileanu, C. Zanni, A. Ferrari, PLUTO: a numerical code for computational astrophysics, Astrophys. J. (2006).

[15] G.L. Brown, A. Roshko, On density effects and large structure in turbulent mixing layers, J. Fluid Mech. 64 (1974) 775–816.

[16] G. Lu, S.K. Lele, On the density ratio effect on the growth-rate of a compressible mixing layer, Phys. Fluids 6 (2) (1994) 1073–1075.

[17] M.D. Slessor, M. Zhuang, P.E. Dimotakis, Turbulent shear-layer mixing: growth-rate compressibility scaling, J. Fluid Mech. 414 (2000) 35–45.

[18] J. Smits, J.P. Dussage, Turbulent Shear Layers in Supersonic Flow, AIP Press, Woodbury, New York, 1996.

[19] P. Colella, P.R. Woodward, The piecewise parabolic method (PPM) for gas-dynamical simulations, J. Comp. Phys. 54 (1) (1984) 174–201.

[20] G.I. Barenblatt, Scaling, Self-Similarity, and Intermediate Asymptotics, Cambridge University Press, 1996, cf. Preface, p. xiii.

[21] A.S. Monin, A.M. Yaglom, Statistical Fluid Mechanics, vol. 1, MIT Press, Cambridge, 1979.

[22] H. Ikawa, T. Kubota, Investigation of supersonic turbulent mixing layer with zero pressure gradient, AIAA J. 13 (1975) 566–572.

[23] R.C. Maydew, J.F. Reed, Turbulent mixing of compressible free jets, AIAA J. 1 (1963) 1443.

[24] M. Sirieix, J.L. Solignac, Contribution à l'étude experimentale de la couche de melange turbulent isobare d'un ecoulment supersonique, in: Separated Flows, AGARD CP4, 1966.